Nuclear Engineering and Technology 54 (2022) 130–137

Contents lists available at ScienceDirect

Nuclear Engineering and Technology

journal homepage: www.elsevier.com/locate/net

Original article

Ignition and flame propagation in hydrogen-air layers from a geological nuclear waste repository: A preliminary study

Je Ir Ryu [a], Seung Min Woo [b, *], Manseok Lee [c], Hyun Chul Yoon [d, **]

[a] Department of Mechanical Engineering, University of California - Berkeley, Berkeley, CA, 94720, USA
[b] Department of Nuclear and Energy Engineering, Jeju National University, Jeju, 63243, Republic of Korea
[c] Goldman School of Public Policy, University of California - Berkeley, Berkeley, CA, 94720, USA
[d] Petroleum & Marine Division, Korea Institute of Geoscience and Mineral Resources, Daejeon, 34132, Republic of Korea

ARTICLE INFO

Article history:
Received 17 February 2021
Received in revised form
24 June 2021
Accepted 10 July 2021
Available online 19 July 2021

Keywords:
Layered flame
Ignition
Flame propagation
Hydrogen
Geological repository
Nuclear waste disposal
Anaerobic corrosion

ABSTRACT

In the geological repository of radioactive nuclear waste, anaerobic corrosion can generate hydrogen, and may conservatively lead to the production of hydrogen-air layer. The accumulated hydrogen may cause a hazardous flame propagation resulting from any potential ignition sources. This study numerically investigates the processes of ignition and flame propagation in the layered mixture. Simple geometry was chosen to represent the geological repository, and reactive flow simulations were performed with different ignition power, energy, and locations. The simulation results revealed the effects of power and energy of ignition source, which were also analyzed theoretically. The mechanism of layered flame propagation was suggested, which includes three stages: propagation into the hydrogen area, downward propagation due to the product gas, and horizontal propagation along the top wall. To investigate the effect of the ignition source location, simulations with eight different positions were performed, and the boundary of hazardous ignition area was identified. The simulation results were also explained through scaling analysis. This study evaluates the potential risk of the accumulated hydrogen in geological repository, and illustrates the layered flame propagation in related ignition scenarios.

1. Introduction

The utilization of nuclear energy confronts the issue of nuclear waste management, particularly, spent nuclear fuel because several isotopes in spent fuel possess long half-life (e.g., I-127: 1.57×10^7 years and Np-237: 2.14×10^6 years), and high toxicity (e.g., Sr-90, Cs-137, and Cs-134). Therefore, a deep geological repository for spent nuclear fuel should be guaranteed with its reliability being as more than tens of thousands of years. For the reliability and safety of a geological disposal, studies for potential criticality events [1–4], as well as environmental [5,6], mechanical [7,8], thermal [9–11], and corrosion [12–15] impacts in the system have been conducted. Among various impacts, it was mentioned that the anaerobic corrosion in the anoxic condition could generate hydrogen based on chemical reactions as follows [14,16,17]:

$$Fe + 2H_2O \rightarrow Fe(OH)_2 + H_2, \quad (1)$$

$$3Fe + 4H_2O \rightarrow Fe_3O_4 + 4H_2, \quad (2)$$

$$3Fe(OH)_2 \rightarrow Fe_3O_4 + 2H_2O + H_2. \quad (3)$$

Anaerobic corrosion is the corrosion of metal by anoxic water. That condition will be reached within a few hundred years after the closure of the geological repository [18].

Various relevant studies have focused on hydrogen in the geological repository [19–24]. For example, in the coated canister, the above reactions can be triggered if the coating is failed. Moreover, the investigated hydrogen evolution rates by the anaerobic corrosion were 2.6×10^{-6} g/h directly from copper in water [19], and up to approximately 60 dm^3/m^2/year directly from carbon steel in artificial groundwater at the temperature of 50 °C [20]. The effect of radiation on the hydrogen generation was also analyzed [21]. The hydrogen gas production in an entire geological repository was numerically simulated in the three-dimension [22]. The authors mentioned that the amount of hydrogen generated in the

* Corresponding author.
** Corresponding author.
E-mail addresses: woosm@jejunu.ac.kr (S.M. Woo), hyun.yoon@kigam.re.kr (H.C. Yoon).

https://doi.org/10.1016/j.net.2021.07.011

geological repository could vary between approximately 10^9 to 10^{10} mol depending on cases and conditions. Moreover, a methodology to model the two-phase flow consisting of the hydrogen gas and liquid water through a porous media was developed and analyzed [23,24].

H_2 generated from canisters by various chemical reactions could be practically kept by the backfill such as bentonite. However, we conservatively assumed the situation that the loss of backfill material or fractures in the backfill material so that H_2 gas can diffuse to the atmosphere of the deep geological repository and precipitate into a crack on that repository. Once more we would like to emphasize that the generation and precipitation of H_2 gas in the deep geological repository is based on the conservative assumption for the study.

When the amount of hydrogen accumulates to a certain level, it may cause a hazardous flame propagation due to potential ignition sources in the geological repository. The modes of flame propagation, such as deflagration and detonation of the homogeneous hydrogen-air mixture in the confined geometry, were numerically investigated [25]. The flame propagation can initiate a detonation from the flame itself or the end-wall boundary, and thus, high pressure rise was observed. The modes of hydrogen-air flame propagation in the inhomogeneous mixture were also studied [26–28], revealing the detailed mechanism of propagation in the concentration gradient layers. As the time scale of hydrogen accumulation in the geological repository is very long, the realistic scenarios may include a highly stratified or layered condition that has distinct separation between hydrogen and air due to the buoyancy effect [29]. investigated the autoignition behavior in the contact layer between the hydrogen-nitrogen mixture and the hot air. However, they focused on the ignition delay in the contact layer and did not consider the flame propagation. To the best of the authors' knowledge, the flame propagation of layered hydrogen-air in geological repository conditions has not been discussed in open literature yet. Therefore, in this study, the flammability and flame propagation by the ignition of layered hydrogen-air are numerically investigated under potential and extreme scenarios for hydrogen distributions and ignition sources.

The remainder of this paper is organized as follows. In Section 2, the methodologies for numerical experiments are addressed. In Section 3, the numerical results are presented with a detailed investigation on the power and energy of ignition source, flame propagation in the layered mixture, and the location of ignition source. The summary and conclusions of the study are found in Section 4.

2. Methodology

Transient three-dimensional reacting flow simulations were performed using CONVERGE software [30]. The software has been utilized in many previous numerical studies (e.g. Refs. [31–35]), and proven to be robust and reliable for reacting flow simulations. Species, momentum, and energy conservation equations were solved through a pressure-implicit with splitting of operators algorithm, and a flux blending finite volume method. A fixed embedding near the hydrogen-air layers and an adaptive mesh refinement method based on temperature and velocity were employed for computational efficiency. The standard k-ε Reynolds-averaged Navier-Stokes model was chosen for turbulence modeling. Moreover, we used a 9-species skeletal chemical kinetic model for hydrogen combustion [36], so the transient rates of species production/consumption and heat release were fully solved coupling with the flow. The minimum grid size was 2.5 mm to resolve the flame propagation behavior with the time step dynamically adjusted to satisfy the Courant–Friedrichs–Lewy conditions. The cell size was determined based on the convergence test.

The geometry of the simulation domain is presented in Fig. 1, which is axisymmetric with respect to the vertical centerline. The cylindrical domain with a radius of 0.5 m and a height of 0.3 m represents the geological repository. The actual size of the geological repository is significantly larger than the current simulation domain. However, only the region near the hydrogen deposition and ignition was considered to reduce the computational cost. The domain size was decided to avoid the flame propagation being affected by the boundary. The cylinder was filled with air. A hemisphere with a radius of 50 mm was placed at the top center of the cylindrical domain to mimic the crack or small hall on the ceiling of the geological repository. Typically, due to the buoyancy effect, the generated hydrogen gas moves to the ceiling of the repository, and if there exists a hole or crack on the ceiling, hydrogen gas is likely to accumulate in there. Therefore, we assumed that the accumulation time was significantly long, so that the hemisphere was filled with hydrogen gas. The initial conditions for both cylinder and hemisphere domains were the standard temperature and pressure (i.e., 298 K and 1 atm), together with wall boundary conditions.

In Fig. 2, the schematic of the simulation setup near the hydrogen deposition region is demonstrated with the slice view at the domain center. The hemisphere center is located at the origin of the coordinate axes ($x = y = z = 0$). Initially, air and hydrogen were completely separated vertically at $z = 0$. The concentration of hydrogen, X_{H_2}, was 1 at $z \geq 0$, and 0 at $z < 0$. The air concentration, X_{air}, was 0 at $z \geq 0$, and 1 at $z < 0$. In the current setup, the amount of accumulated hydrogen in the hemisphere is 21.42 mg, which is several orders of magnitude smaller than that from a typical geological repository per year [18].

The size of the ignition source was set to be on the order of magnitude of a typical spark plug gap. Here, the ignition source was spherical with a radius of 2.5 mm for all simulation cases. Our main goal is to elucidate the effect of ignition source on the layered flame. Particularly, we focus on the effect of ignition power, energy, and location. The regime of ignition is identified, and the flame propagation mechanism is explained.

3. Results and discussion

3.1. Power and energy of ignition source

In a geological repository of radioactive nuclear waste, accumulated hydrogen during a long period of time can cause catastrophic accidents as mentioned in the earlier section. Typically, the ambient temperature in the repository is below the autoignition temperature of hydrogen at 1 atm in air, 673 K [37]; thus, the

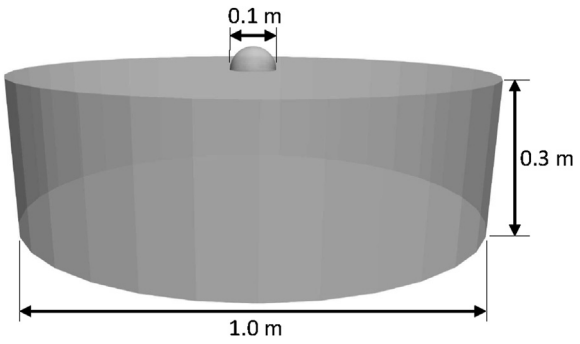

Fig. 1. Geometry of the simulation domain.

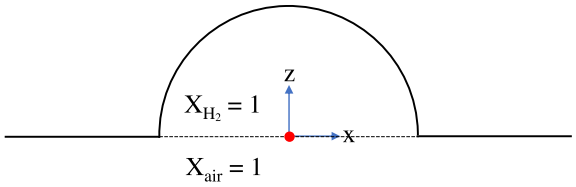

Fig. 2. Schematic of simulation setup in a slice view. The dashed line indicates the hydrogen-air interface.

accumulated hydrogen does not self-ignite. However, even with a small amount of energy source such as a spark from bulbs, cables, fans, etc., the combustion of hydrogen can be initiated and sustained after the ignition source is removed. For example, a ringing telephone caused an accident in the Three Mile Island (TMI) Unit 2 [38].

In a homogeneous stoichiometric premixed hydrogen/air mixture, the minimum ignition energy can be estimated by integrating the lumped form of the energy conservation equation over the ignition duration with assumptions of spherical energy source and negligible combustion heat [37]:

$$E_{ign} = \rho c_p V(T_f - T_i) + Q_{loss}, \quad (4)$$

where, E_{ign}, V, Q_{loss} are the energy of ignition source, volume of energy source, and heat loss to the ambient mixture, respectively. ρ, c_p, T_f, and T_i indicate the density, specific heat, ignition temperature, and initial temperature of hydrogen/air mixture, respectively. The ignition temperature can be estimated from the autoignition delay time. In actual scenarios, the ignition duration is significantly short, i.e., on the order of 0.1–1 ms. If the time scale of ignition delay is much longer than that of ignition duration, the effect of Q_{loss} may be significant, and thus, the hydrogen/air mixture fails to ignite. For hydrogen/air stoichiometric mixture, the ignition delay is on the order of 0.1 ms at approximately 1000 K, while it is on the order of 10–100 ms at 900 K, from zero-dimensional ignition delay calculations using SENKIN [39]. Therefore, the minimum required ignition temperature is ~1000 K to have a negligible heat loss term compared to other terms, so that the mixture can ignite. Then, the rough estimation for the minimum ignition energy from Equation (4) is ~0.06 J for a spherical ignition source with a radius of 2.5 mm.

For simulations, a spherical ignition source with a radius of 2.5 mm was imposed initially at the origin of the coordinate axes, i.e., the ignition source includes hydrogen and air in the upper and lower hemispheres, respectively. Due to the separation of hydrogen and air, the ignition behavior may be different from that of the homogeneous case. To investigate the effect of the ignition source power, we fixed the amount of energy to 0.1 J and varied ignition duration, Δt, from 0.5 ms to 5 ms. The maximum temperature profiles are presented in Fig. 3, which are up to 10 ms for the cases with ignition duration times of 0.5, 1.0, 2.0, 3.0, 4.0, and 5.0 ms to depict the ignition behaviors. It can be observed from the figure that the maximum ignition duration is between 2.0 and 3.0 ms, while the corresponding power being 55 and 33 W, respectively. For the case with ignition duration of 2.0 ms, the temperature became slightly higher than 1000 K during the heating by the ignition source, then the mixture was ignited in the order of 0.1 ms. When $\Delta t = 3.0$ ms, the ignition source cannot heat the mixture sufficiently (~870 K); thus, the mixture failed to ignite due to a large amount of heat loss to the ambient mixture. These processes agree with the rough estimation using ignition delay.

Although the minimum ignition energy can be estimated from Equation (4) for the homogeneous mixture, the ignition behavior may differ in the layered mixture. The maximum temperature

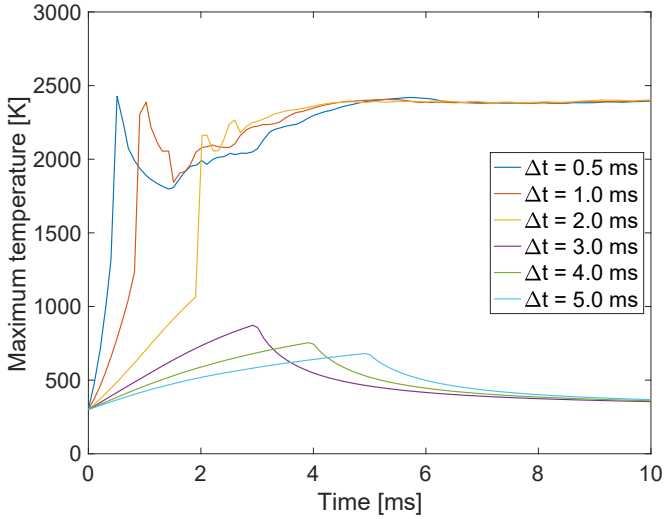

Fig. 3. Maximum temperature profiles when the amount of ignition source energy is 0.1 J with various ignition duration times of 0.5, 1.0, 2.0, 3.0, 4.0, and 5.0 ms.

profiles with different ignition energy from 0.05 to 0.10 J, with the ignition duration being fixed to 0.5 ms, are shown in Fig. 4. The threshold for the ignition is between 0.07 and 0.08 J. The ignition energy of 0.07 J did not increase mixture temperature higher than 1000 K during the source heating; thus, the mixture did not ignite, and temperature decreased after the source heating due to heat transfer to the outside. For the cases with $E_{ign} \geq 0.08$ J, the mixtures were sufficiently heated and ignited by the ignition source.

The results reveal that the accumulated hydrogen can be ignited although it is layered with air. The amount of power required is approximately 40 W, which corresponds to a small light bulb, and the threshold for the energy is only 0.08 J, which is similar to the value estimated from the lumped energy conservation equation.

3.2. Flame propagation in layered mixture

For the feasible simulation of flame propagation in the layered mixture, the energy deposition in the source was 0.1 J for 0.5 ms at $x = y = z = 0$ (Case 1). The simulation result with slice views of

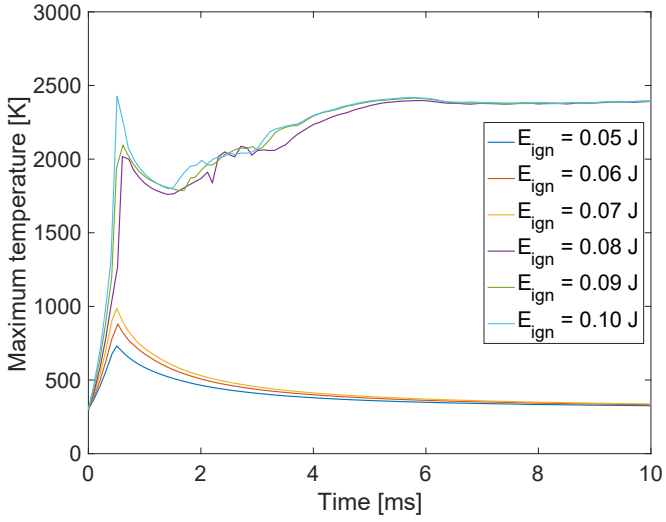

Fig. 4. Maximum temperature profiles when the ignition duration is 0.5 ms with various amounts of ignition energy 0.05, 0.06, 0.07, 0.08, 0.09, and 0.10 J.

several time sequences at the center is presented in Fig. 5. The ignition source is located at the hydrogen-air layer and the center of the hemisphere. Left figures represent temperature distribution at the middle plane, while the middle and right figures show the distributions of hydrogen and oxygen, respectively. Note that the time sequence intervals are not even to demonstrate the propagation phenomena clearly.

At 5 ms, the energy deposition produces ignition and a temperature rise near the ignition location. The ignition kernel is not perfectly spherical due to the layered configuration of the mixture and buoyancy effect. Ideally, the layered mixture is not likely to ignite as the oxygen and hydrogen gases are separated. However, if the energy deposit is at the layer interface, it can be ignited due to the local mixing of fuel and air. Moreover, the heated air mixture moves into the hydrogen gas due to the buoyancy effect as shown in oxygen concentration at 5 ms. Thus, the shape of the

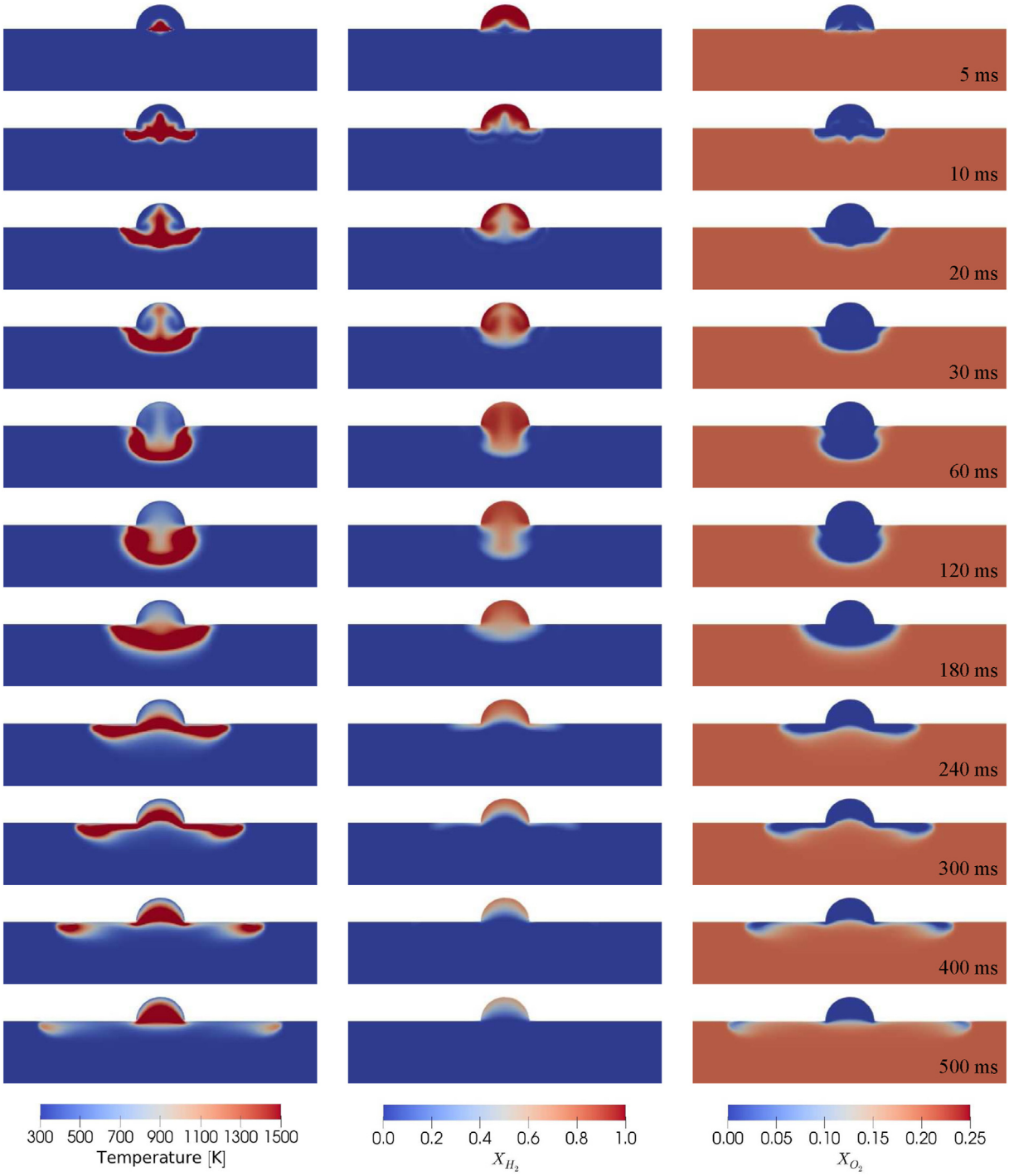

Fig. 5. Slice views of temperature, X_{H_2}, and X_{O_2} at 5, 10, 20, 30, 60, 120, 180, 240, 300, 400, and 500 ms from the simulation result with an ignition source of 0.1 J for 0.5 ms at $x = y = z = 0$.

flame kernel is a triangle, which propagates along with the hydrogen-air interface and inside of the hydrogen region until approximately 30 ms.

Once the air near the hydrogen is consumed by the combustion process, the hydrogen gas comes out from the hemisphere to the cylindrical region. The product of the combustion (i.e., water vapor) has higher temperature and volume, so it pushes the hydrogen gas to the outside of the hemisphere. Then, the pushed hydrogen gas contacts the air again; thus, the flame can further propagate to the downward until ~120 ms. However, some amount of hydrogen is still at the top of the hemisphere and does not ignite as the gas is completely separated from the air.

After ~120 ms, the ejected hydrogen is ignited outside the hemisphere, with the product of combustion located at the bottom of the hemisphere. The flame and its product go up with expansion, so the hydrogen gas is pushed and ejected along the hemisphere wall and the top wall of the cylindrical domain due to the buoyancy effect. The flame now propagates along the top wall of the cylindrical domain while the center of flame moves into the hemisphere until ~300 ms. Then, when the flame center and its product completely cover the interface between the hemisphere and cylinder, the hydrogen cannot be ejected any longer, so the flame along the top wall of the cylinder is detached from the center and disappeared at approximately 500 ms.

Overall, in the layered flame, there exist three ignition stages as shown above. In the first stage, the flame kernel starts to propagate with the triangle shape in the hemisphere. Then, the product of combustion pushes hydrogen gas to the downward, with the flame propagates to the downward in the second stage. In the last stage, the flame goes back to the hemisphere due to the buoyancy effect and it pushes the hydrogen along the top wall of the cylinder; thus, the flame also propagates along the top wall.

3.3. Location of ignition source

Simulations with eight different ignition source locations as shown in Table 1 were performed to elucidate the effect of the ignition source location. The locations were set to investigate how the interaction between ignition source and buoyancy affected the flame propagation. For all cases, the energy depositions in the source were 0.1 J for 0.5 ms. Case 1 is the reference case in which the ignition source is located at $x = y = z = 0$ as in the previous section. Cases 2 and 3 have different horizontal locations, while ignition sources are located between the hydrogen and air layers vertically. The ignition sources on the left side ($x < 0$) were not considered as the domain is axisymmetric, and the results should be the same as in cases with ignition sources on the right side. Cases 4–7 have different vertical locations, so the ignition sources are either in the hydrogen or air layer, while the horizontal locations are fixed to the center. The ignition source of Case 8 is off from $x = y = z = 0$ both vertically and horizontally. The location is in the lower boundary of the ignition which will be identified in the latter part of this section, but outside of the horizontal right corner of the hemisphere.

Table 1
Locations of ignition source.

Case number	x [mm]	z [mm]
1	0	0
2	5	0
3	10	0
4	0	−10
5	0	−5
6	0	5
7	0	10
8	55	−5

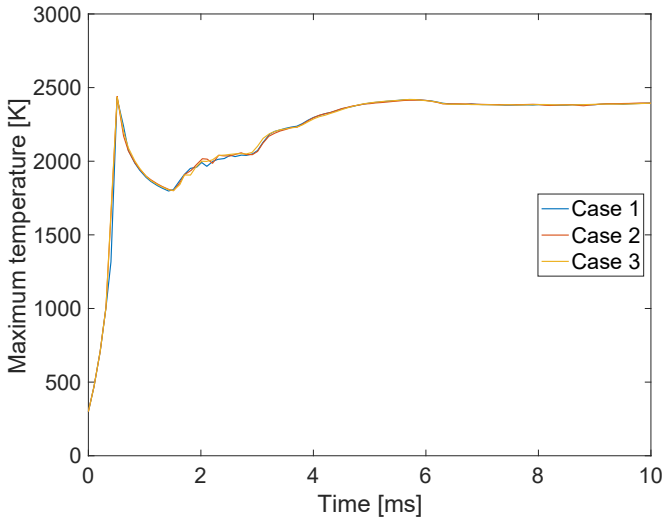

Fig. 6. Maximum temperature profiles for Cases 1, 2, and 3 (ignition source at $x = 0$, 5, and 10 mm, $z = 0$ mm).

The simulation results from Cases 1, 2, and 3 are presented in Fig. 6. The maximum temperature profiles of each case are presented. All cases are ignited regardless of the horizontal location. The ignition behaviors are almost identical. However, the flame propagation patterns may vary due to the different geometric constraints.

The flame propagation of Case 3 is presented in Fig. 7. The three stages of layered flame propagation mechanism can also be observed in Case 3. However, the flame is not propagated symmetrically, and product mixture movement by the buoyancy is different from Case 1. Initially, as the vertical location of ignition source is the same as Case 1, the similar triangle flame kernel can be observed at 5 ms. The kernel also propagates along with the hydrogen-air interface, and inside of the hydrogen area until 30 ms, but the shape of kernel is not symmetrical due to the different boundary effect. When the hydrogen gas comes out from the hemisphere to the cylindrical region, it is deflected to the $x > 0$ side until approximately 120 ms. Then, the ejected hydrogen is burnt at the bottom of the hemisphere and propagated along the top wall of cylindrical region. Unlike to Case 1, the flame center and its product do not cover the interface between the hemisphere and cylinder symmetrically. The $x < 0$ side is less covered by the product as the flame kernel is located more on the $x > 0$ side. Thus, the detached flame along the top wall of the cylinder in the $x < 0$ side is sustained longer than that of Case 1.

The effect of vertical ignition source location is presented in Fig. 8. If the vertical ignition location, z, is −10, 5, or 10 mm, the flame is not propagated. The ignition source is too far from the interface; thus, either the amount of hydrogen or oxygen is not enough to ignite. If the mixture is not ignited during the energy deposit, the temperature increase is limited, so the fluid dynamics effect by the buoyancy is not initiated.

For the case with $z = 5$ and 10 mm, even though the energy deposit initially increases the adjacent temperature, it will not produce any ignition as the required oxygen cannot be provided. Therefore, the energy deposit should touch the interface between the hydrogen and air to initiate ignition:

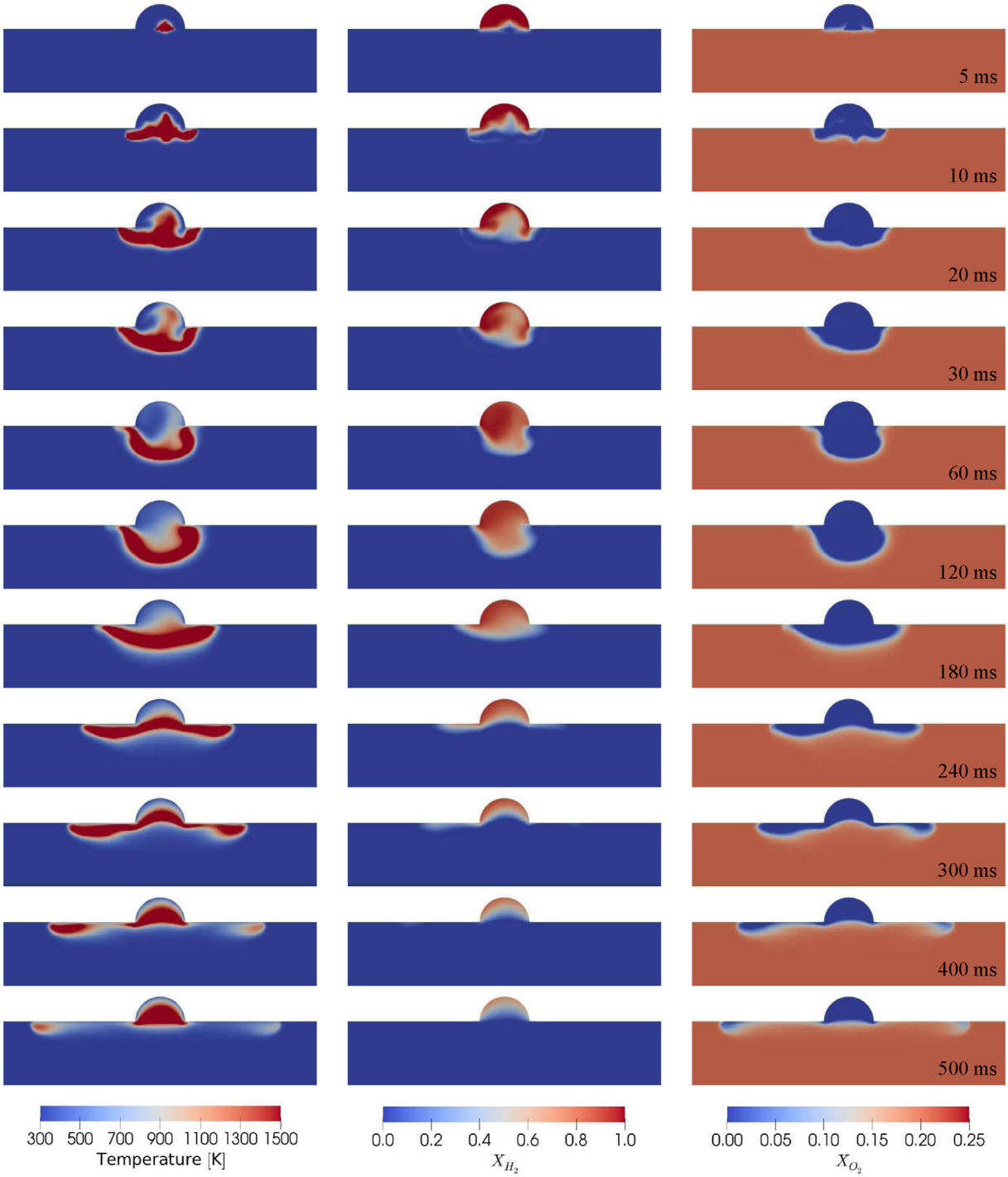

Fig. 7. Slice views of temperature, X_{H_2}, and X_{O_2} at 5, 10, 20, 30, 60, 120, 180, 240, 300, 400, and 500 ms from Case 3 simulation result.

$$z < r_E, \tag{5}$$

where, r_E is the radius of initial energy deposition. Here, r_E is 2.5 mm.

If the ignition location is below the interface between hydrogen and air, e.g., $z = -5$ and -10 mm, ignition may be initiated with sufficient levels of temperature and distance to the hydrogen interface. Although the initial high-temperature sphere does not contain any hydrogen to ignite, the hydrogen can be heated by several mechanisms. The size of the high-temperature sphere becomes larger due to the thermal expansion, while the heat is transferred outside of the sphere due to the conduction. In Fig. 8, the temperature of Case 5 increases up to approximately 1600 K during the energy deposition. Then, the maximum temperature decreases due to the thermal expansion and heat transfer to the outside. At approximately 0.6 ms, the expended hot sphere touches the hydrogen boundary while the temperature is still sufficiently high (~1460 K), so the hydrogen/air mixture can ignite spontaneously. Case 4 follows a similar mechanism to Case 5

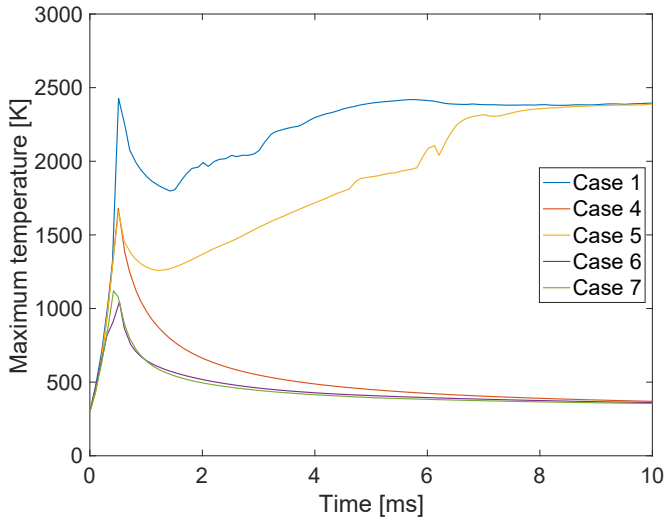

Fig. 8. Maximum temperature profiles for Case 1 and Cases 4–7 (ignition source at $x = 0$ mm, $z = 0$, −10, −5, 5, and 10 mm).

initially. However, it takes longer for the expended hot sphere to touch the hydrogen boundary as the ignition source is located further down; thus, the temperature is not sufficiently high to ignite the mixture.

In the current setup, it is reasonable to estimate the ignition time scale to the order of 1 ms, based on the ignition duration. To have an ignition delay on the order of 1 ms, a stoichiometric hydrogen-air mixture requires approximately 1000 K of mixture temperature. If the temperature does not exceed certain level, the mixture fails to ignite, due to the amount of heat loss being larger than the heat release rate. From the 0.1 J of energy deposit in the radius of 2.5 mm for 0.5 ms, the temperature can be increased approximately 1600 K. The high-temperature sphere is extended due to the thermal expansion. When the radius becomes ~1.85 times of the original radius, the temperature in the extended high-temperature sphere is approximately 1000 K. If the hot sphere expands further, the temperature is insufficient to ignite within the ignition time scale. Therefore, another criterion for the vertical location of the ignition source can be established as follows:

$$z > -1.85 r_E. \tag{6}$$

From the scaling analysis, the length scale, l_{conv}, for conductive heat transfer process can be estimated as:

$$l_{cond} \sim \sqrt{\tau\alpha}, \tag{7}$$

where, τ is the time scale of the process, which is 1 ms, and α is the thermal diffusivity. Thus, the estimated length scale is on the order of 0.1 mm, which is negligible compared to the thermal expansion length scale.

The velocity of the hot sphere in the $+z$-direction by buoyancy force, u, can be scaled using the governing equation of the fluid motion due to the effect of buoyancy [40] as:

$$u \sim \sqrt{l_b g \beta (T_h - T_\infty)}, \tag{8}$$

where, l_b, g, β, T_h, and T_∞ indicate the buoyancy length scale, gravitational acceleration, volume expansion coefficient, temperature of the hot sphere, and ambient temperature, respectively. Here, u is on the order of 0.1 m/s. During the ignition time scale, the amount of hot sphere movement in $+z$-direction is on the order of 0.1 mm, which can also be neglected.

Therefore, the overall criterion for the vertical location is:

$$-1.85 r_E < z < r_E, \tag{9}$$

in which, the upper and lower bounds are 2.5 mm and −4.6 mm, respectively. In the real case, the temperature distribution in the expanded hot sphere may not be homogeneous, and the temperature in the upper part may be higher than that in the lower part. Then, the lower bound can be extended further as the larger expended hot sphere can still have a sufficiently high temperature to ignite in the ignition time scale. Considering the effect of inhomogeneous temperature distribution in the hot sphere, the simulation results exhibit a good agreement with the criterion developed as above. Moreover, the limit can be extended if the layered mixture is partially stratified. Once ignition starts, the layered flame follows the same stages as described in the previous section: propagation into the hydrogen area, downward propagation due to the product gas, and horizontal propagation along the top wall.

Case 8 does not ignite although it satisfies the criterion for the vertical location. The top of the hot sphere touches the $z = 0$ plane, but it does not have an interface with the accumulated hydrogen as it is outside the hydrogen hemisphere.

4. Conclusions

The ignition and flame propagation of the hydrogen-air layered mixture in the geological repository of radioactive nuclear waste were investigated using numerical simulations. The effects of ignition source power, energy, and location were presented, and the flame propagation mechanism was introduced. The following conclusions are drawn:

- The simulation results demonstrate the effect of power and energy of ignition source. Both theoretical and numerical results show that the minimum ignition power and energy are approximately 40 W and 0.08 J, respectively, for a spherical ignition source with a radius of 2.5 mm.
- The mechanism of layered flame propagation was suggested based on the simulation results. In the first stage, the flame kernel starts to propagate with the triangle shape in the hemisphere. Then, the product of combustion pushes hydrogen gas downward, so the flame propagates to that direction. In the last stage, the flame returns to the hemisphere due to the buoyancy effect and it pushes the hydrogen along the top wall of the cylinder; thus, the flame propagates along the top wall.
- To investigate the effect of the ignition source of horizontal and vertical locations, simulations with eight different points were performed. The biased horizontal location induced the asymmetric flame propagation and longer sustained flame kernel. The vertical boundary of the hazardous ignition location was identified by the scaling analysis. The upper bound is the radius of the ignition source sphere, while the lower bound is approximately twice of the source radius due to the thermal expansion, buoyancy movement, and heat conduction. The criterion corresponds to the simulation results.

This study suggests the potential riskiness of the accumulated hydrogen in the geological repository, and depicts the layered flame propagation in the ignition scenarios. For broader applications, different geometries should be investigated, and the hydrogen accumulation process should also be further studied. Moreover,

experimental validation of H_2 generation and its combustion process in the deep geological repository will be essential.

Declaration of competing interest

The authors declare that they have no known competing financial interests or personal relationships that could have appeared to influence the work reported in this paper.

Acknowledgments

This work was supported by the research grant of Jeju National University in 2020. Moreover, the authors would like to appreciate Convergent Science for providing SMW with CONVERGE license and support.

References

[1] C.D. Bowman, F. Venneri, Underground Autocatalytic Criticality from Plutonium and Other Fissile Material, Tech. Rep. LA-UR-94-4, Los Alamos National Laboratory, Los Alamos, New Mexico, 1995.
[2] J. Ahn, Criticality safety assessment for a conceptual high-level-waste repository in water-saturated geologic media, Nucl. Technol. 126 (3) (1999) 303–318, https://doi.org/10.13182/NT99-A2976.
[3] J. Ahn, E. Greenspan, P.L. Chambré, A preliminary consideration for underground autocatalytic criticality by vitrified high-level waste in water-saturated geologic repository, J. Nucl. Sci. Technol. 37 (5) (2000) 465–476, https://doi.org/10.1080/18811248.2000.9714919.
[4] X. Liu, J. Ahn, F. Hirano, Conditions for criticality by uranium deposition in water-saturated geological formations, J. Nucl. Sci. Technol. 52 (3) (2014) 416–425, https://doi.org/10.1080/00223131.2014.953616.
[5] J. Ahn, An environmental impact measure for nuclear fuel cycle evaluation, J. Nucl. Sci. Technol. 41 (3) (2004) 296–306, https://doi.org/10.1080/18811248.2004.9715488.
[6] J. Ahn, Environmental impact of Yucca Mountain Repository in the case of canister failure, Nucl. Technol. 157 (1) (2007) 87–105, https://doi.org/10.13182/NT07-A3804.
[7] Y.J. Kwon, J.W. Choi, Finite element stress analysis of spent nuclear fuel disposal canister in a deep geological repository, JSME International Journal Series A Solid Mechanics and Material Engineering 46 (4) (2003) 543–549, https://doi.org/10.1299/jsmea.46.543.
[8] A.K. Verma, P. Gautam, T.N. Singh, R.K. Bajpai, Discrete element modelling of conceptual deep geological repository for high-level nuclear waste disposal, Arabian Journal of Geosciences 8 (2015) 8027–8038, https://doi.org/10.1007/s12517-014-1762-7.
[9] L.H. Johnson, M. Niemeyer, G. Klubertanz, P. Siegel, P. Gribi, Calculations of the Temperature Evolution of a Repository for Spent Fuel, Vitrified High-Level Waste and Intermediate Level Waste in Opalinus Clay, Tech. Rep. 01-04, National Cooperative for the Disposal of Radioactive Waste, Wettingen, 2002.
[10] J.Y. Lee, D.K. Cho, H.J. Choi, J.W. Choi, L.M. Wang, Analyses of disposal efficiency based on nuclear spent fuel cooling time and disposal tunnel/pit spacing for the design of a geological repository, Prog. Nucl. Energy 53 (2011) 361–367, https://doi.org/10.1016/j.pnucene.2011.01.005.
[11] W.-J. Cho, J.-S. Kim, H.-J. Choi, Hydrothermal modeling for the efficient design of thermal loading in a nuclear waste repository, Nucl. Eng. Des. 276 (2014) 241–248, https://doi.org/10.1016/j.nucengdes.2014.06.005.
[12] F. King, Overview of a Carbon Steel Container Corrosion Model for a Deep Geological Repository in Sedimentary Rock, Tech. Rep. TR-2007-01, Nuclear Waste Management Organization, Toronto, Ontario, 2007.
[13] F. King, Critical Review of the Literature on the Corrosion of Copper by Water, Tech. Rep. SKB-TR-10-69, Swedish Nuclear Fuel and Waste Management Co., Solna, 2010.
[14] N.R. Smart, Corrosion behavior of carbon steel radioactive waste packages: A summary review of Swedish and UK research, Corrosion 65 (3) (2009) 195–212, https://doi.org/10.5006/1.3319128.
[15] B. Kursten, F. Druyts, D.D. Macdonald, N.R. Smart, R. Gens, L. Wang, E. Weetjens, J. Govaerts, B. Kursten, F. Druyts, D.D. Macdonald, N.R. Smart, R. Gens, L. Wang, E. Weetjens, J. Govaerts, Review of corrosion studies of metallic barrier in geological disposal conditions with respect to Belgian Supercontainer concept, Corrosion Engineering, Sci. Technol. 46 (2) (2011) 91–97, https://doi.org/10.1179/1743278210Y.0000000022.
[16] U.R. Evans, J.N. Wanklyn, Evolution of hydrogen from ferrous hydroxide, Nature 162 (4105) (1948) 27–28, https://doi.org/10.1038/162027b0.
[17] J. Jelinek, P. Neufeld, Kinetics of hydrogen formation from mild steel in water under anaerobic conditions, Corrosion 38 (2) (1982) 98–104, https://doi.org/10.5006/1.3577332.
[18] T. Xu, R. Senger, S. Finsterle, Corrosion-induced gas generation in a nuclear waste repository: reactive geochemistry and multiphase flow effects, Appl. Geochem. 23 (12) (2008) 3423–3433, https://doi.org/10.1016/j.apgeochem.2008.07.012.
[19] G. Hultquist, Hydrogen evolution in corrosion of copper in pure water, Corrosion Sci. 26 (2) (1986) 173–177, https://doi.org/10.1016/0010-938X(86)90044-2.
[20] N.R. Smart, D.J. Blackwood, L. Werme, The Anaerobic Corrosion of Carbon Steel and Cast Iron in Artificial Groundwaters, Tech. Rep. SKB-TR-01-22, Swedish Nuclear Fuel and Waste Management Co., Solna, 2001.
[21] N.R. Smart, A.P. Rance, L.O. Werme, The effect of radiation on the anaerobic corrosion of steel, J. Nucl. Mater. 379 (2008) 97–104, https://doi.org/10.1016/j.jnucmat.2008.06.007.
[22] J. Brommundt, T.U. Kaempfer, C.P. Enssle, G. Mayer, J. Wendling, Full-scale 3D modelling of a nuclear waste repository in the Callovo-Oxfordian clay. Part 1: thermo-hydraulic two-phase transport of water and hydrogen, Geological Society 400 (1) (2014) 443–467, https://doi.org/10.1144/SP400.34.
[23] A. Bourgeat, M. Jurak, F. Smaï, Two-phase, partially miscible flow and transport modeling in porous media; application to gas migration in a nuclear waste repository, Comput. Geosci. 13 (1) (2009) 29–42, https://doi.org/10.1007/s10596-008-9102-1.
[24] B. Amaziane, M. Jurak, A.Ž. Keko, Modeling and numerical simulations of immiscible compressible two-phase flow in porous media by the concept of global pressure, Transport Porous Media 84 (1) (2010) 133–152, https://doi.org/10.1007/s11242-009-9489-8.
[25] X. Shi, J.I. Ryu, J.-Y. Chen, R.W. Dibble, Modes of reaction front propagation and end-gas combustion of hydrogen/air mixtures in a closed chamber, Int. J. Hydrogen Energy 42 (15) (2017) 10501–10512, https://doi.org/10.1016/j.ijhydene.2016.12.095.
[26] J.I. Ryu, Detonation Initiation, Propagation, and Suppression, Ph.D. thesis, University of California, Berkeley, 2018.
[27] J. I. Ryu, X. Shi, J.-Y. Chen, Numerical study of detonation propagation in fuel-stratifiaction layers, Manuscript submitted for publication.
[28] J.I. Ryu, X. Shi, J.-Y. Chen, Modes of detonation wave propagation in water vapor concentration gradients, Combust. Sci. Technol. 192 (10) (2020) 1910–1930, https://doi.org/10.1080/00102202.2019.1630615.
[29] H.G. Im, J.H. Chen, C.K. Law, Ignition of hydrogen-air mixing layer in turbulent flows, Symposium (International) on Combustion 27 (1) (1998) 1047–1056, https://doi.org/10.1016/S0082-0784(98)80505-5.
[30] Convergent Science, CONVERGE (2.4) [computer program], 2019. Available at: https://convergecfd.com [Accessed 31 October 2019].
[31] Y. Chen, T. Chen, Y. Feng, J.I. Ryu, H. Yang, J.-Y. Chen, H radical sensitivity-assisted automatic chemical kinetic model reduction for laminar flame chemistry retaining: A case study of gasoline-DME mixture under engine conditions, Energy Fuels 33 (4) (2019) 3551–3556, https://doi.org/10.1021/acs.energyfuels.8b04282.
[32] J.I. Ryu, A.H. Motily, T. Lee, R. Scarcelli, S. Som, K.S. Kim, C.-B.M. Kweon, Ignition enhancement of F-24 jet fuel by a hot surface for aircraft propulsion systems, in: AIAA Scitech 2020 Forum, 2020, https://doi.org/10.2514/6.2020-2142.
[33] J.I. Ryu, A.H. Motily, T. Lee, R. Scarcelli, S. Som, K.S. Kim, C.-B.M. Kweon, Ignition of jet fuel assisted by a hot surface at aircraft compression ignition engine conditions, in: 2020 AIAA Propulsion and Energy Forum, 2020, https://doi.org/10.2514/6.2020-3889.
[34] A.H. Motily, J.I. Ryu, K. Kim, K.S. Kim, C.-B.M. Kweon, T. Lee, High-pressure fuel spray ignition behavior with hot surface interaction, Proc. Combust. Inst. 38 (4) (2021) 5665–5672, https://doi.org/10.1016/j.proci.2020.08.041.
[35] J.I. Ryu, A.H. Motily, T. Lee, R. Scarcelli, S. Som, K.S. Kim, C.-B.M. Kweon, Effect of hot probe temperature on ignition of alcohol-to-jet (ATJ) fuel spray under aircraft propulsion system conditions, in: AIAA Scitech 2021 Forum, 2021, https://doi.org/10.2514/6.2021-0985.
[36] M.P. Burke, M. Chaos, Y. Ju, F.L. Dryer, S.J. Klippenstein, Comprehensive H2/O2 kinetic model for high-pressure combustion, Int. J. Chem. Kinet. 44 (7) (2012) 444–474, https://doi.org/10.1002/kin.20603.
[37] S. McAllister, J.-Y. Chen, A.C. Fernandez-Pello, Fundamentals of Combustion Processes, 2011.
[38] OECD Nuclear Energy Agency, Flame Acceleration and Deflagration-To-Detonation Transition in Nuclear Safety, Tech. Rep. NEA/CSNI/R(2000)7, OECD Nuclear Energy Agency, Issy-les-Moulineaux, 2000.
[39] A.E. Lutz, R.J. Kee, J.A. Miller, SENKIN: A Fortran Program for Predicting Homogeneous Gas Phase Chemical Kinetics with Sensitivity Analysis, Tech. Rep. SAND87-8248, Sandia National Laboratories, Livermore, CA, 1988.
[40] Y.A. Cengel, Heat Transfer: A Practical Approach, second ed., McGraw-Hill, 2003.